Hydrogen dissociation in a H_2-N_2 pulsed dc glow discharge

James M. Williamson[1] and Biswa N. Ganguly[2]
[1]*Innovative Scientific Solutions, Inc., 2766 Indian Ripple Road, Dayton, Ohio 45440-3638*
[2]*Air Force Research Laboratory, Wright-Patterson Air Force Base, Ohio 45433-7919*
(Received 10 January 2000)

The absolute concentration of hydrogen atoms is measured in the positve column of a pulsed dc discharge by two-photon absorption laser-induced fluorescence in H_2 and H_2-N_2 gas mixtures at constant pressure and current. The discharge pulse duration is varied from 10 μsec to 1 msec. For shorter pulse durations of 10 and 100 μsec, the H-atom signal decreased monotonically with H_2 concentration; for longer pulse durations of $\geqslant$500 μsec, the fractional dissociation of the H_2 is enhanced with increasing N_2 concentration. The change in H-atom production from direct electron impact dissociation of H_2 at short times compared to that from multiquantum vibrational energy transfer induced dissociation of H_2 at long times is determined from temporally resolved H-atom concentration measurements.

PACS number(s): 52.20.Hv, 52.70.Kz, 52.80.Hc

I. INTRODUCTION

Molecular gas discharges in N_2 and H_2-N_2 gas mixtures are commonly applied in metal surface nitriding [1–5], while H_2 discharges are used for surface treatments, e.g., cleaning, passivation, and etching, in the Si and GaAs semiconducter industries [6–8]. These applications have prompted numerous studies on gas discharges of both pure H_2 and N_2 [1,9–15] as well as discharges of H_2-N_2 gas mixtures [2,3,5,16–27], the aim being to elucidate the details of these plasmas. Compared to rare gas or single molecular gas discharges, discharges in molecular gas mixtures are further complicated by heavy particle energy exchange processes as well as direct electron impact processes [2,21,22].

The addition of a small percentage of H_2 to a N_2 discharge substantially increases the dissocitation of N_2 [21]; similarly the addition of a small percentage of N_2 to a H_2 discharge increases the H_2 dissociation [20]. Nagpal *et al.* [22] measured the absolute dissociation efficiency of H_2 in a H_2-N_2 gas mixture discharge and, from their analysis of the energy balance, showed that the H_2 was dissociated via a multiquantum ($\delta v \geqslant 18$) vibrational energy transfer mechanism with vibrationally excited ground electronic state N_2 ($X\,^1\Sigma_g^+, v$). Measurements of the fractional dissociation efficiency of D_2 in a D_2-N_2 discharge revealed the same high degree of dissociation of D_2, demonstrating that the H_2 and D_2 could be dissociated by a similar multiquantum vibrational energy transfer mechanism with N_2 ($X\,^1\Sigma_g^+, v$) [25].

The aim of this study was to further investigate the heavy-particle energy transfer dissociation of H_2 in a H_2-N_2 gas discharge by examining the H atom production in temporally resolved, pulsed discharges rather than steady-state dc or rf discharges. The H atoms produced in the pulsed dc discharges were measured by two-photon absorption laser-induced fluorescence (TALIF) [28]. A high-voltage constant current pulser with variable pulse duration was used to excite the discharge. By varying the discharge pulse duration from a short time regime where the H_2 is dissociated by direct electron impact to a long time regime where the discharge approaches steady-state conditions [3,21,23], the heavy-particle energy transfer contribution to H-atom production relative to direct electron impact was examined.

II. EXPERIMENTAL DETAILS

A schematic diagram of the experimental apparatus is shown in Fig. 1. The main components of the apparatus are the discharge cell, the electronics, and the probe laser system. The discharge cell is a cylindrical glass cell, roughly 37 cm in height and 7.5 cm in diameter. Two sets of opposed windows (diameter 5 cm), orthogonal to each other, are located roughly 25 cm from the bottom of the cell; one set of windows permits passage of the laser through the cell, and the other allows viewing of the laser-excited fluorescence or plasma emission. The laser entrance and exit windows are made of high-quality fused silica and the fluorescence-viewing windows are made of BK-7. The cell is evacuated through 3.5 cm i.d. glass and metal lines by an Alcatel 5010 drag pump, backed with an oil-free diaphragm pump. With

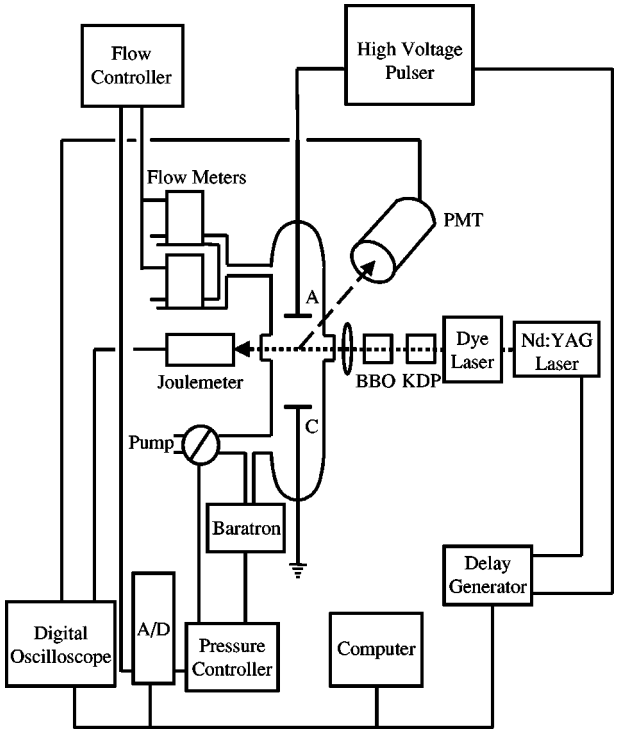

FIG. 1. Schematic diagram of the experimental apparatus.

no gas flowing, the system pumps down to <1 mTorr.

The discharge gas flows were controlled with flow controllers (MKS Type 1259 flow controller) and an MKS Type 247C four-channel readout, while the cell pressure was maintained by a control valve and an exhaust valve controller (MKS Types 253A and 252, respectively). The cell pressure was measured with a baratron pressure gauge (MKS Type 102A) whose output was sent to the valve controller for maintaining a constant pressure in the discharge cell. The gas flow could be varied from 0 to 100 SCCM (SCCM denotes cubic centimeters per minute at STP), and the baratron pressure gauge operated in the range 0–10 Torr. The gases were externally mixed, after the flow controllers, and entered at the top of the cell through an internal glass-tubing loop with evenly spaced 1 mm holes. Both the H_2 and N_2 discharge gases were obtained from Matheson (UHP grade, 99.999%).

The discharge electrodes were two aluminum discs 5 cm in diameter with an interelectrode spacing of 7 cm. The discharge voltage was provided by a current-regulated, pulsed power supply. The current was adjustable to 1.5 A, and the voltage was adjustable to 12 kV. The pulse width could be adjusted from 5 μsec to 1.1 msec, with pulse rise and fall times of less than 0.5 μsec (with a 5kΩ ballast resistor) and a repetition rate of single shot to 20 Hz.

The measurement of atomic hydrogen via TALIF has been detailed elsewhere [20,28]. In brief, the output of a *Q*-switched, Nd:YAG-pumped (where YAG is yttrium aluminum garnet) dye laser (Quanta-Ray DCR-2A, PDL-3) near 615 nm (SR-640 dye) was frequency doubled in a temperature stabilized potassium dihydrogen phosphate (KDP) crystal. The resulting uv radiation was then mixed with the dye fundamental in a β-barium borate (BBO) crystal to generate the 205 nm radiation for exciting atomic hydrogen from the $1s$ to the $3s,3d$ states. The Balmer α emission (656.3 nm) from the excited hydrogen was detected at right angles to the laser and the electrode axis by a Hamamatsu R1477 photomultiplier tube (PMT). The residual 205 nm probe radiation was measured by a Molectron Model J3-05 power meter after exiting the discharge cell. Probe pulse energies were typically 200–300 μJ.

The fluorescence was collected through an iris diaphragm by a focusing lens and passed through a narrow bandpass filter centered at 656 nm (3 nm full width at half maximum) and neutral density filters. The iris diaphragm reduced the background signal due to scattered laser light from the windows, while the neutral density filters eliminated saturation of the PMT due to the large plasma-induced emission during the discharge pulse. The PMT output was amplified and sent to a digital oscilloscope (LeCroy 9354C) for signal capture and averaging, while the laser power-meter output was also sent to the oscilloscope. The averaged PMT signal and laser power-meter signal were finally sent to a PC for signal processing.

The hydrogen-atom TALIF measurements were performed with a cell pressure of 2.5 Torr, a total gas flow rate of 40 SCCM, and a constant discharge current of 250 mA. The cell pressure, gas flow rate, and gas mixture were computer controlled. The duration of the discharge pulse was varied from 10 μsec to 1 msec and synchronized with the laser probe pulse by a Stanford Research DG535 delay generator, which was also computer controlled. The hydrogen atoms were probed 20 μsec after the discharge pulse was turned off.

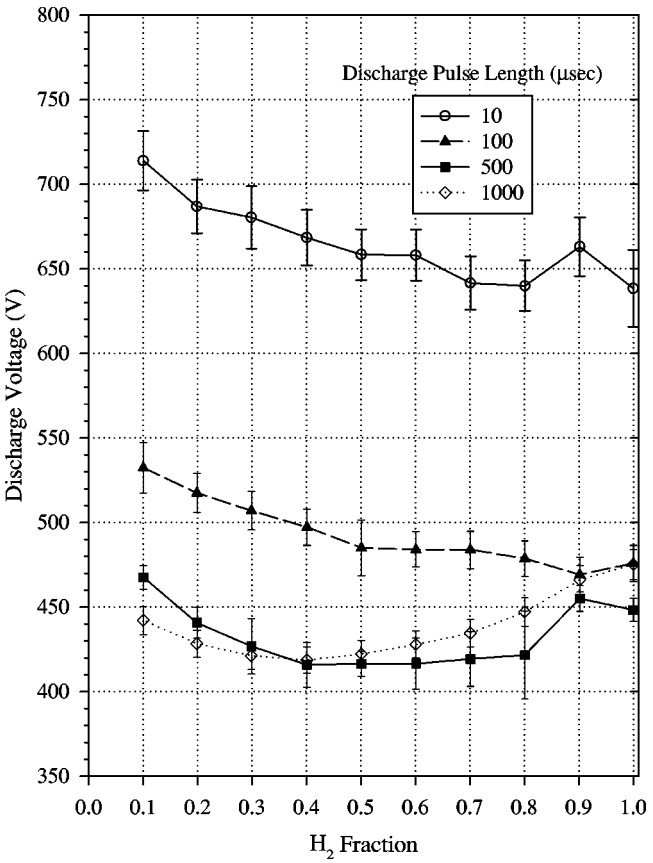

FIG. 2. H_2-N_2 discharge voltage as a function of gas mixture and discharge pulse duration. H_2 fraction is the fractional flow of H_2 in the H_2-N_2 gas mixture. Cell pressure, total gas flow, and discharge current were 2.5 Torr, 40 SCCM, and 250 mA, respectively.

III. RESULTS

Variation of the measured discharge voltage with H_2 fraction in the gas mixture for four discharge pulse durations is shown in Fig. 2 for a cell pressure of 2.50 Torr and a discharge current of 250 mA. The discharge voltage can be seen to vary only slightly ($<10\%$) with H_2 fraction in the gas mixture over the entire range of H_2 fraction in the gas mixture. The volume electric field was determined as a function of gas mixture, with a movable gap spacing for a cell pressure of 2.50 Torr and a discharge current of 250 mA. The fixed anode electrode used for the TALIF experiments was replaced with a movable electrode assembly. The movable and fixed electrodes were the same diameter and made of the same material. The electrode gap spacing was incrementally changed, with a 7 cm gap as the midpoint of the electrode travel, and the discharge voltage was measured after each gap spacing change with a high-voltage probe. Plots of the discharge voltage as a function of electrode gap spacing were linear. Slopes of these curves, with 7 cm being the center point, determined the volume electric field. The determined electric fields in gas mixtures of 10–100 % H_2 in H_2-N_2 for the different discharge pulse durations are shown in Fig. 3.

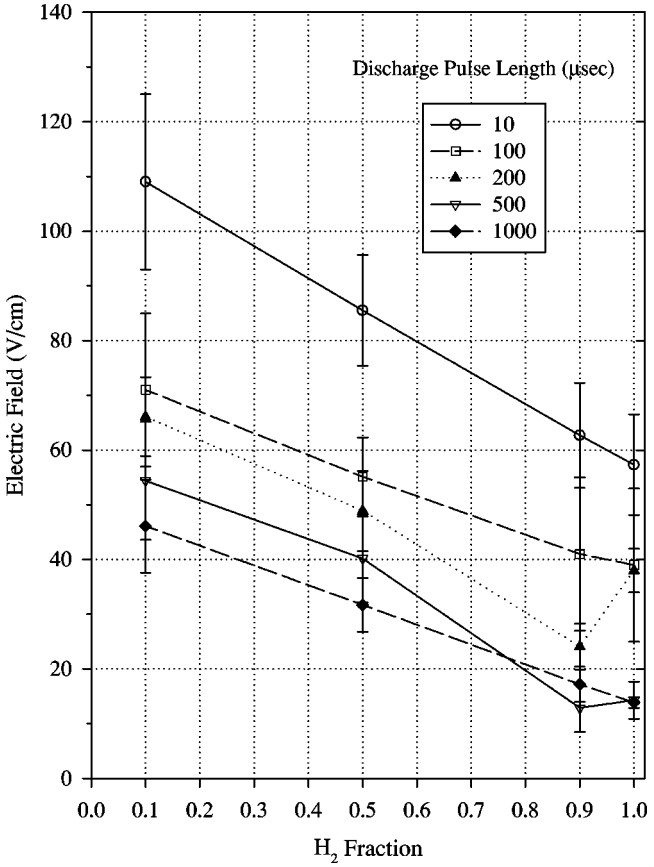

FIG. 3. Determined volume electric field in a H_2-N_2 discharge using movable gap spacing. Discharge conditions were the same as in Fig. 2.

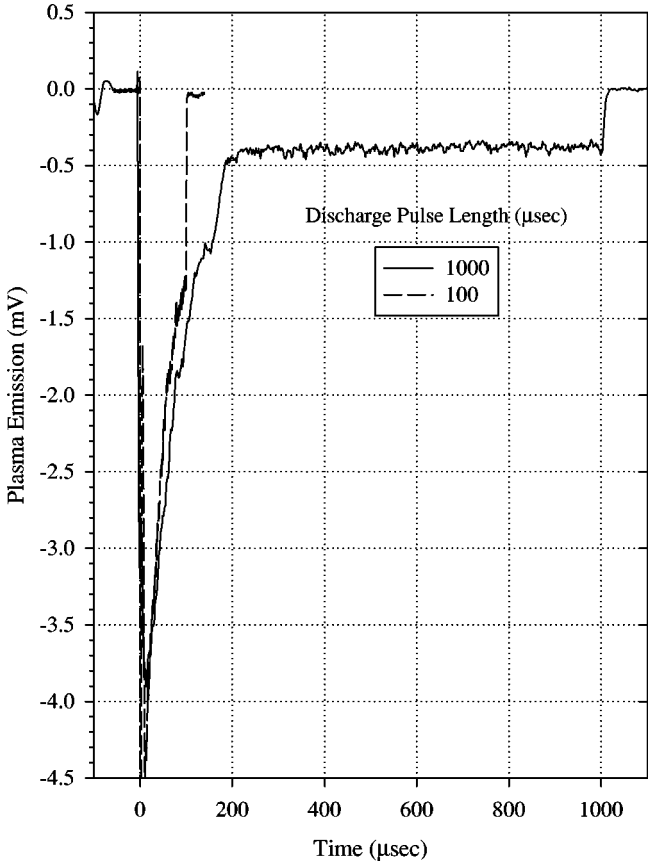

FIG. 4. H_α plasma emission in a H_2 discharge for 100 and 1000 μsec discharge pulses. Discharge conditions were the same as in Fig. 2.

In general, the electric field is highest for the shortest discharge pulse (10 μsec) and decreases with pulse duration. The electric fields for the 500 and 1000 μsec discharge pulses are lower than those for the 100 and 200 μsec pulses because of gas heating [18,19].

The determined electric fields in Fig. 3 for pulse durations of 10, 100, and 1000 μsec monotonically increase with N_2 dilution (i.e., decreasing H_2 fraction in the gas mixture). The shape of these curves is in agreement with calculations of the electric field [17–19,26] and with electric field measurements [19] in H_2-N_2 gas mixtures; the electric field increases with decreasing H_2 fraction in the H_2-N_2 gas mixture. The electric fields for 200 and 500 μsec pulses as a function of H_2 fraction in the gas mixture exhibit behavior that is different from that for the 10, 100, and 1000 μsec pulses. The electric field decreases with the initial addition of N_2 before monotonically increasing with decreasing H_2 fraction in the gas mixture. The decrease in electric field at 90% H_2 is greater for the 200 μsec discharge pulse than for the 500 μsec pulse. This initial decrease in the electric field with the addition of N_2 is not present in the calculations [18,19,26]. The reason for this decrease in the electric field is not clear, and at present we have no explaination for this dip in the electric field.

Along with the volume electric field, the background plasma emission viewed by the PMT through the 656 nm bandpass filter, corresponding to H_α, was recorded. The background plasma emission for 100 and 1000 μsec discharge pulses in a pure H_2 discharge is shown in Fig. 4. The emission for the 1000 μsec pulse (solid curve) shows an initial burst of H_α emission in the first 200 μsec, followed by a constant level for the remainder of the discharge pulse. The 100 μsec pulse (dashed curve) has the same shape as the first 100 μsec of the longer 1000 μsec pulse before shutting off at 100 μsec. The H_α emission for all pulse durations used has the same temporal shape and can be visualized by truncating the 1000 μsec pulse in Fig. 4 at the appropriate time (as in the case of the 100 μsec pulse shown in Fig. 4). From the determined volume electric field, E/n values (where E is the electric field and n is the number density) can be estimated. The plasma emission decreases with pulse duration up to 200 μsec as does the electric field; thus, for the shorter discharge pulses, it is assumed that gas heating is negligible and the number density does not change. At longer times (200–1000 μsec), the electric field decreases, but the plasma emission is constant. This implies that E/n remains constant from 200 to 1000 μsec and that the number density is lower because of gas heating [18,19].

The relative H-atom signals were measured as a function of H_2 fraction in a H_2-N_2 gas mixture at a constant pressure and discharge current as described above. Since it is known that H-atom fluorescence is quenched more by N_2 than by H_2 [29], it was necessary to examine the temporal decay of the H-atom fluorescence for different mixtures of H_2 in N_2 under the same discharge conditions used for the relative H-atom measurements. The H-atom TALIF fluorescence signal wave forms for 100%, 50%, and 20% H_2 in H_2-N_2 gas mixtures

along with a PMT signal wave form of the 6-nsec probe laser (scattered from a spot at the focal point of the collection optics) were recorded. The temporal profiles of the H-atom fluorescence signal wave forms were the same for all the gas mixtures and slightly broader than the scattered light wave form, indicating that the fluorescence decay time was the same in the gas mixtures. The decay time of the signal wave forms obtained from a semilogarithmic plot confirmed that the lifetime of the fluorescence decay for the different gas mixtures was the same. (Note that similar behavior was reported previously [20].) Since no difference was observed in the fluorescence decays for gas mixtures of 0–80 % N_2 in H_2-N_2, no quenching correction was applied to the relative H atom signals as a function of N_2 fraction.

To ensure that the plasma emission background signal would not obscure the H-atom TALIF fluorescence signal, the H atoms were probed after the discharge pulse was turned off. Although the plasma emission was attenuated by neutral density and narrowband bandpass filters, an emission signal at 656 nm from both H_α and the N_2 first positive emission was still viewed by the PMT. This interference from the background plasma emission signal to the H-atom TALIF signal was reduced by measuring the TALIF signal 20 μsec after the discharge pulse was turned off (at a delay of 20 μsec after the discharge was turned off, there was virtually no plasma emission signal for any of the H_2 fractions in H_2-N_2 gas mixtures used). To verify that the H atom TALIF signal did not change from the time the discharge was turned off to the time the H atom was probed, the temporal behavior of the signal was measured. Figure 5 shows the H-atom TALIF signal in the time interval 10–200 μsec after a 500 μsec discharge pulse was turned off for gas mixtures of 100%, 80%, 50%, and 20% H_2 in N_2. It is apparent that the signal was nearly constant over this period and did not change during the 20 μsec time delay after the discharge pulse. In the same way, the H-atom TALIF signal was measured for all the discharge pulse durations used; the signal did not change for this period for any pulse duration.

Hydrogen dissociation in the mixed-gas discharge was initially measured with short duration discharge pulses—10 and 100 μsec (at constant current). The relative H-atom TALIF signal as a function of H_2 fraction in the H_2-N_2 gas mixture for these short duration pulses is shown in Fig. 6. Although the relative signal level is lower for the shorter duration discharge pulse (note that the signal has been magnified five times in Fig. 6), the two curves are essentially the same; the relative H-atom signals decrease monotonically with increasing N_2 fraction in the gas mix. The relative H-atom TALIF signals for longer duration discharge pulses, 200 and 1000 μsec, along with the 100 μsec data, are also shown in Fig. 6. The shapes of the relative signal curves for the longer duration discharge pulses are not the same as those for the short pulses. The H-atom signal initially decreases with the addition of N_2 then increases with further addition until it levels off for 10–60 % H_2 in the gas mix for the 1000 μsec duration pulse; for the 200 μsec pulse, the signal initially decreases and then increases with the addition of N_2, as in the case of the 1000 μsec pulse, but then decreases after reaching a maximum at 60–70 % H_2. The nearly constant H-atom signal for the 1000 μsec pulse with 10–60 % H_2 indicates that the fractional dissociation of H_2 is increasing with N_2 concentration with the longer pulse.

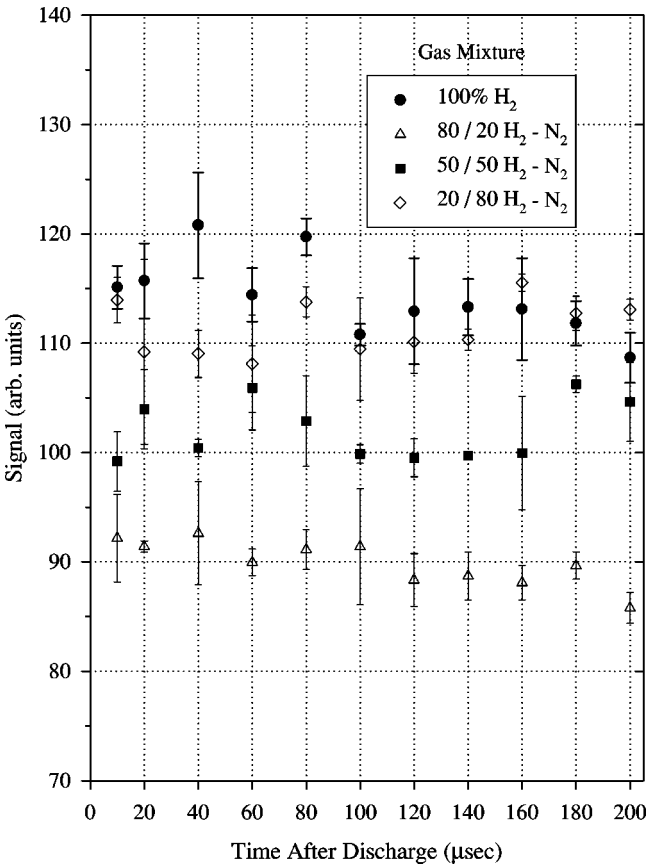

FIG. 5. H-atom TALIF signal in a H_2-N_2 discharge as a function of time after the discharge pulse was turned off for various gas mixtures. Gas compositions are indicated on the graph. Discharge conditions were the same as in Fig. 2.

IV. DISCUSSION

The relative H-atom TALIF signal was calibrated to an absolute number density using the calculated fractional power deposition into H_2 dissociation in a pure H_2 discharge [22] and the experimentally determined E/n values. The fractional power deposited into different inelastic modes—electronic, vibration, rotation, and dissociation—was calculated by Nagpal *et al.* [22] for H_2, N_2, and specific H_2-N_2 mixtures as a function of E/n. The fractional energy density deposited into H_2 dissociation with the discharge conditions used here for the pure H_2 discharge was calculated from the determined E/n values and the calculated fractional power deposited into H_2 dissociation. The absolute H-atom number density for each discharge pulse duration used was then determined from the calculated energy density, assuming an energy dissipation of 10 eV in H_2 dissociation. (The thermal dissociation energy of H_2 is $\sim$4.5 eV, while the threshold for H_2 dissociation by electron impact is $\sim$9 eV. Thus the use of 10 eV—which is just above threshold but approximately twice the dissociation energy—would mean that the calculated number densities would be at most low by a factor of 2.) The calculated absolute H-atom number density along

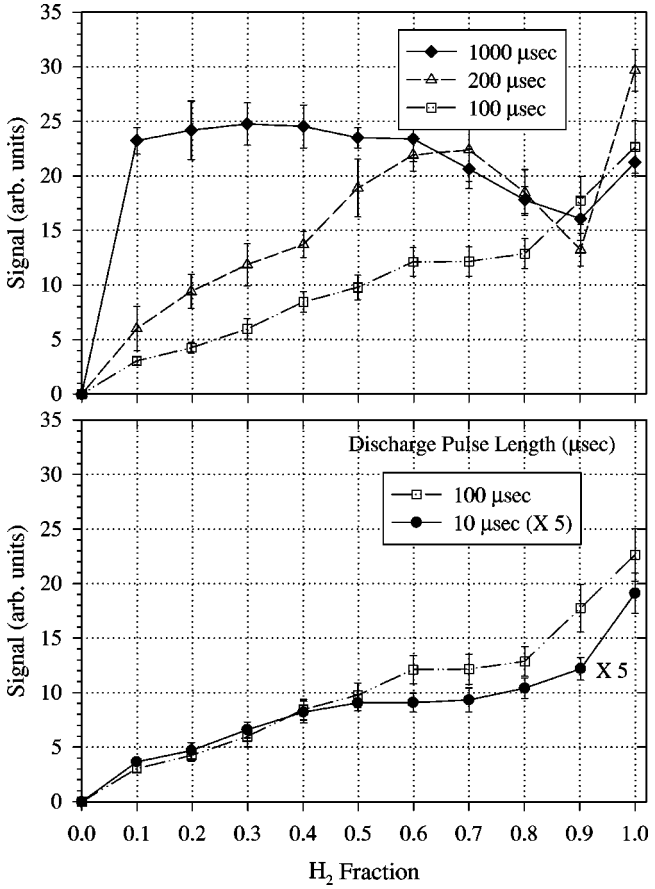

FIG. 6. Relative H-atom TALIF signal as a function of discharge pulse duration. Discharge conditions were the same as in Fig. 2. Note that the signal for the 10 μsec discharge pulse (bottom graph) has been multiplied by 5 to facilitate comparison with the 100 μsec pulse signal.

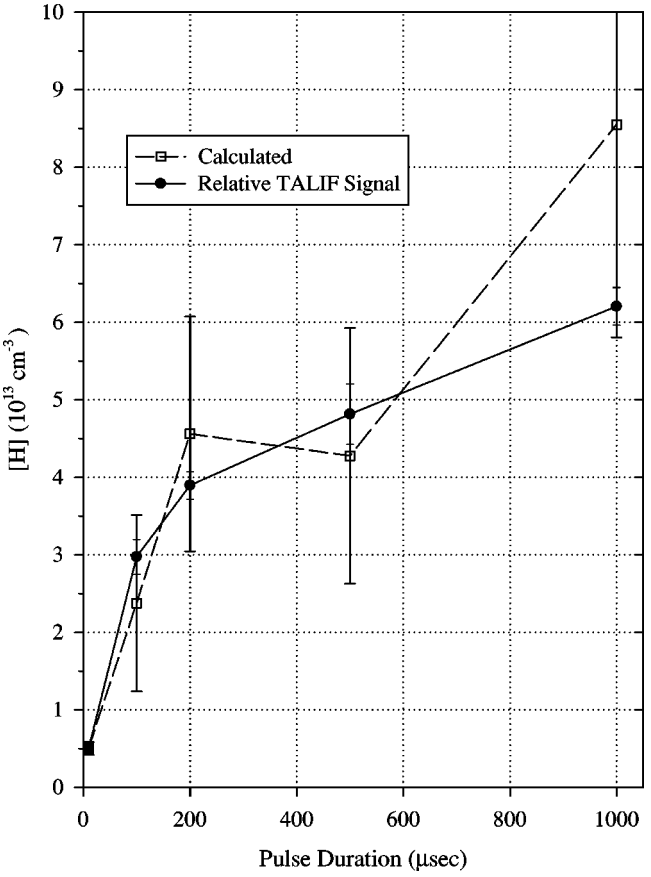

FIG. 7. H-atom TALIF signal calibration for a H_2 discharge from power deposition calculation. Open squares are calculated densities and closed circles are experimental TALIF signals. Relative TALIF signals were scaled to the calculated densities at the 10 μsec data points.

with the electric field, E/n values, and fractional power deposited into dissociation is summarized in Table I. It should be noted that because of gas heating during the longer (500 and 1000 μsec) discharge pulses, as discussed previously, the E/n values were assumed to remain constant for discharge pulses $\geqslant$200 μsec.

The relative H-atom TALIF signal for a pure H_2 discharge was then calibrated to the calculated H-atom densities derived from the fractional power deposition calculations by normalizing the TALIF signal of the 10 μsec discharge pulse to the corresponding calculated absolute density. Since gas heating should be negligible for a 10 μsec discharge pulse, the gas number density will not be affected by any temperature rise in the constant pressure discharge. The H-atom TALIF signals for the other discharge pulse durations were then scaled from the TALIF signal for the 10 μsec pulse. Although the TALIF signals were roughly constant for the first 200 μsec after the discharge pulse was turned off (see Fig. 5), the signal level did decay exponentially for longer times after the discharge pulse was turned off (the decay was measured up to 10 msec after the discharge was turned off). The TALIF signal for the 500 and 1000 μsec discharge pulses was corrected for this long-time

TABLE I. Volume electric field, E/n values, energy densities, and absolute H-atom densities calculated from fractional power deposition in a H_2 discharge.

t (μsec)	E (V/cm)	E/n (Td)[a]	P (W/cm^3)	%P[b]	E_H (10^{-6} J/cm^3)	[H] (10^{13} cm^{-3})
10	57±9	70±11	0.73±0.11	54±4	4.0±0.7	0.50±0.08
100	39±14	48±17	0.50±0.18	38±12	19.0±0.9	2.4±1.2
200	38±14	47±5	0.48±0.05	38±12	36.5±1.2	4.4±1.4
500	14±3	47±10	0.18±0.004	38±12	34.2±1.3	4.2±1.6
1000	14±3	47±10	0.18±0.01	38±12	68.4±2.2	8.4±2.8

[a]1 Townsend (Td)=10^{-17} V cm^2.

[b]Fractional power deposition in H_2 dissociation from Ref. [22].

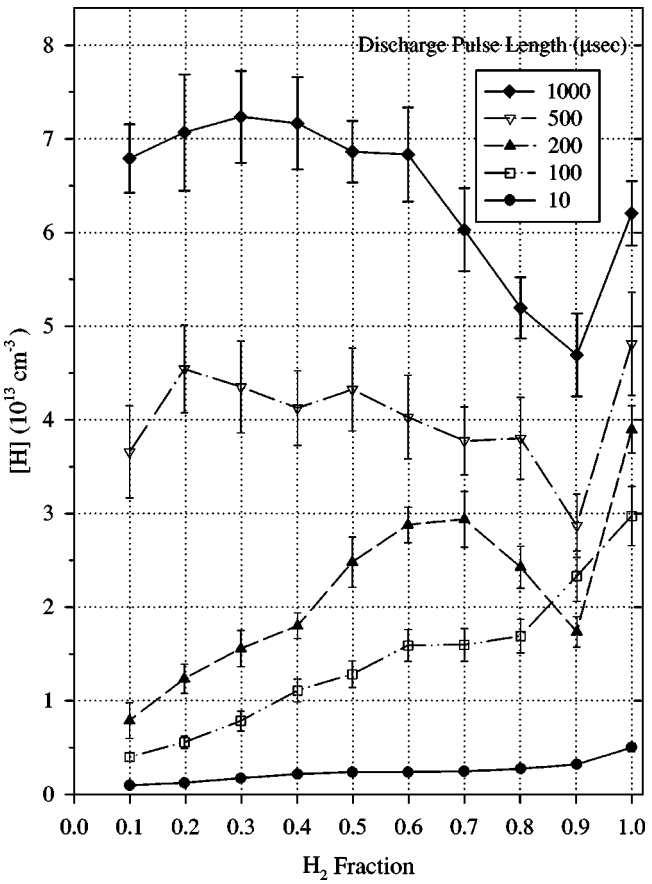

FIG. 8. Absolute H-atom density as a function of gas mixtures for different discharge pulse durations in a H_2-N_2 discharge.

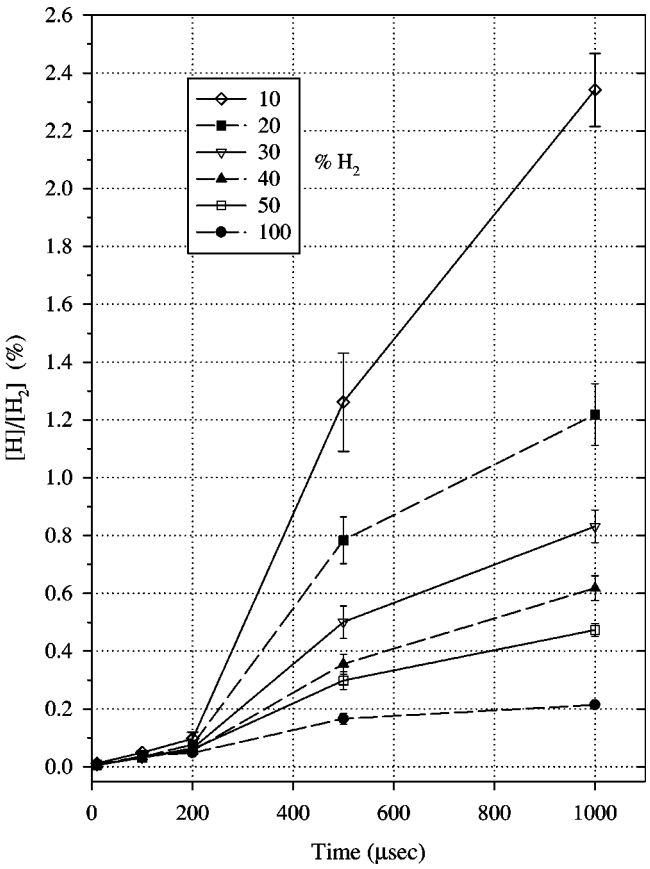

FIG. 9. Fractional H_2 dissociation as a function of discharge pulse durations for different gas mixture in a H_2-N_2 discharge.

decay by multplying the TALIF signal level by a correction factor that grew exponentially with the inverse time constant of the measured decay rate before being scaled to the absolute number density. The calibrated H-atom TALIF signals and calculated H-atom number densities for a pure H_2 discharge are shown in Fig. 7. The scaled TALIF signal is observed to be in reasonable agreement with the calculated H-atom densities.

The relative H-atom TALIF signals as a function of gas mixture and discharge pulse duration were then calibrated from the absolute H-atom densities of the pure H_2 discharge of Fig. 7. The calibrated H-atom densities are shown in Fig. 8. The increased fractional H_2 dissociation with N_2 addition for the longer discharge pulses, 500 and 1000 μsec, is evident in the figure from the nearly constant H-atom density in the range 10–60 % H_2. In contrast, for the shorter pulses, the atom densities decline monotonically with N_2 addition. The enhancement of fractional H_2 dissociation with pulse duration and N_2 is evident in Fig. 9 where the H-atom density (as a percentage of H_2 in the H_2-N_2 gas mixture) is shown as a function of pulse duration and gas mixture. For discharge pulses up to 200 μsec, the increase with pulse length is small and no dependence on N_2 concentration is observed. However, for the longer discharge pulses (500 and 1000 μsec), where heavy-particle collisions become significant, the increase in the fractional dissociation of H_2 with N_2 dilution is large, indicating the increase in heavy-particle collision-induced dissociations.

Enhancement in the fractional dissociation of H_2 with the addition of N_2 in a discharge is well known [16,20,21,24]. The previous studies were conducted under steady-state conditions; in the present study the pulsed discharge used allowed examination of the temporal evolution of the H_2 dissociation in the H_2-N_2 discharge. At 10 μsec, the H_2 is dissociated by direct electron impact since insufficient time is available for energy buildup and transfer by heavy-particle collisions [30,31]. Similarily, the H-atom signal for the 100 μsec pulse suggests that H_2 is dissociated by direct electron impact since the shapes of the H-atom signal curve for the 100 μsec pulse and the 10 μsec pulse are essentially the same. This is also evident from the fractional dissociation of H_2 in Fig. 9 where no change occurs in the H-atom signal with N_2 concentration for 10 and 100 μsec.

The H-atom signal for the 500 and 1000 μsec discharge pulses indicates an enhancement in the fractional dissociation of H_2 with increasing N_2 concentration. The H_2 fractional dissociation increases with N_2 concentration for these longer pulses. As shown previously, this increase in fractional H_2 dissociation cannot be caused by direct electron impact [17,20,30] since the majority of the power deposited in a H_2-N_2 discharge is deposited into vibrational and electronic excitation of N_2 [18,22]. The increase in fractional H_2 dissociation is due to energy transfer collisions with electronically and vibrationally excited N_2 [24]. Under continuous discharge conditions, a detailed analysis of the power deposition in a H_2-N_2 discharge showed that although some

contribution from electronically excited N_2 was made to dissociating H_2, it could not account for the experimentally observed fractional dissociation enhancement [16,22]. The major contributer to the dissociation of H_2 was vibrationally excited N_2 ($X\,^1\Sigma_g^+, v \geqslant 18$) [22,24,25]. The temporal evolution of the vibrational excitation of N_2 in a pure N_2 discharge by vibrational energy transfer up-pumping [32,33] was calculated by Gorse and Capitelli [31]. However, comparing the determined H-atom density at 1000 μsec for 10% H_2 in the H_2-N_2 gas mixture with the calculated value of the $N_2, v \geqslant 18$, density at 1000 μsec, the calculated buildup for these high vibrational levels is not sufficiently fast to account for the measured H-atom density. If the H atoms are produced by a multiquantum energy transfer from vibrationally excited N_2, the vibrational population of N_2 in $v \geqslant 18$ must be at least the same as the H-atom density. The calculated $N_2, v = 18$, population is three orders of magnitude lower than the measured H-atom density. Note that the calculation was for slightly different discharge conditions—higher E/n value [60 Td (1 Td$=10^{17}$ V cm^2)] and pressure (5 Torr) versus $E/n \sim 40$ Td and 2.5 Torr pressure in the experiment. Thus, the buildup of N_2 vibrational excitation would be expected to be slightly more rapid in the calculation then in the experiment; although the addition of 10% H_2 to a N_2 steady-state dc discharge increases the midrange vibrational populations ($v \approx 10$–25) in N_2 [18], those populations are only increased by a factor of ~ 5–10. The density is still much less than the observed H-atom density. Thus, in contrast to steady-state conditions where the calculated equilibrium densities in excited N_2 vibrational levels are many orders of magnitude higher [22], it appears that vibrationally excited N_2 alone is not responsible for the fractional enhancement in the H_2 dissociation.

N_2 can be vibrationally excited in a discharge by vibrational energy transfer up-pumping, and calculations have shown that H_2 can also be vibrationally excited by the same processes [10,34]. Another possible mechanism of H-atom production is multiquantum energy transfer dissociation of vibrationally excited H_2 from vibrationally excitated N_2. The calculation of Loureiro and Ferreira [10] showed that the buildup of vibrational population in N_2, $v \sim 8$–10, was comparable to the H-atom density measured for a 1000 μsec pulse. The H_2 would have to be excited to the $v=4$ and 5 levels to possess sufficient energy to be dissociated by vibrational energy transfer from N_2, v$=10$ and 8, respectively. Although a complete self-consistent theoretical calculation of the vibrational energy transfer up-pumping in the discharge is beyond the scope of the present study, the trend in the time evolution of the vibrational up-pumping in H_2 can be examined, and the population in excited vibrational levels $v=4$ and 5 in H_2 can be estimated for comparison to the H-atom density.

The heavy-particle vibrational energy transfer kinetics can be modeled by solving a set of vibrational master equations that account for vibration-to-vibration and vibration-to-translation collisional energy exchanges [10,18,26]. The temporal evolution of the H_2 vibrational population densities was calculated by integrating a set of differential equations of the form

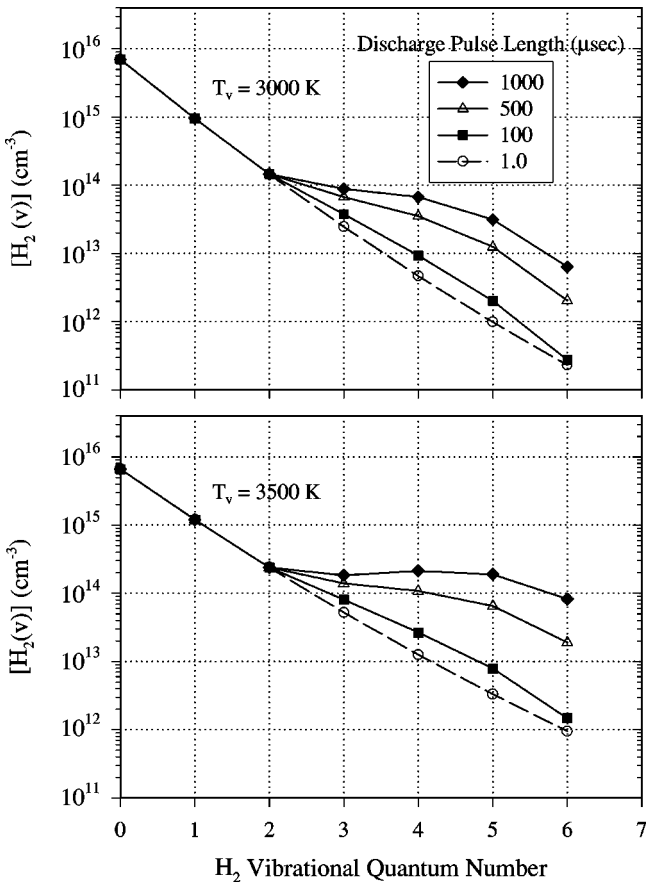

FIG. 10. Temporal evolution of the H_2 vibrational populations for 10% H_2 in a H_2-N_2 discharge for two initial vibrational temperatures. The top graph is for an initial vibrational temperature $T_v = 3000$ K while the lower graph is for $T_v = 3500$ K.

$$\frac{d[\mathrm{H}_2(v)]}{dt} = \sum_{v=0-6} K_{V\text{-}V}^{\mathrm{H}_2,\mathrm{N}_2} n_{\mathrm{H}_2} n_{\mathrm{H}_2,\mathrm{N}_2} - \sum_{v=0-6} K_{V\text{-}T}^{\mathrm{H}_2,\mathrm{H}} n_{\mathrm{H}_2} n_{\mathrm{H}_2,\mathrm{H}}, \quad (1)$$

where $K_{V\text{-}V}^{\mathrm{H}_2,\mathrm{N}_2}$ are the rate constants for vibration-to-vibration energy transfer from H_2 or N_2 to H_2, $K_{V\text{-}T}^{\mathrm{H}_2,\mathrm{H}}$ are the rate constants for vibration-to-translation energy transfer for H_2 or H atoms colliding with H_2, and n_X is the density of H_2, N_2, or H atoms. The vibrational level dependent rate constants were taken from Loureiro and Ferreira [10] and Gordiets *et al.* [26] and calculated for a gas temperature of 400 K. The calculation was for 10% H_2 in H_2-N_2 and limited to $v = 0$–6 in H_2 and $v=0$ in N_2. The initial vibrational distributions in H_2 and N_2 were assumed to be Boltzmann, with a vibrational temperature of either 3000 or 3500 K, i.e., two calculations were performed—one with an initial vibrational temperature (T_v) of 3000 K and the other with T_v of 3500 K. (The average T_v derived from the H_2, $v = 0$–2, vibrational population densities calculated by Cacciatore *et al.* [34] in a pure H_2 discharge and similar discharge conditions was ~ 3700 K.) The calculations were further simplified by fixing the vibrational populations in H_2, $v = 0$–2, and N_2, $v = 0$, at their initial values; only the populations in H_2, v

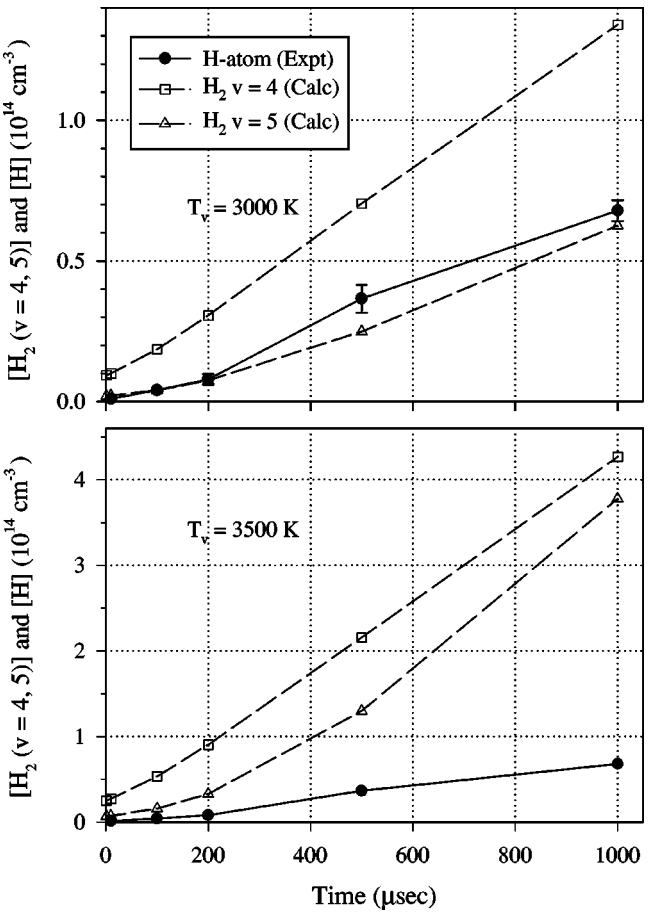

FIG. 11. Comparison of the calculated temporal evolution of $H_2, v=4$ and 5, vibrational populations for two initial vibrational temperatures with the experimental H-atom densities. Experimental H-atom densities are indicated by solid circles; calculated $H_2, v=4$ and 5, densities are indicated by open squares and triangles, respectively. H_2 vibrational densities from Fig. 10 are multiplied by 2 for comparison with the H-atom densities.

$=3$–6, changed with time. The experimentally measured H-atom densities were used in the V-T quenching calculation.

The temporal evolutions of the H_2 vibrational populations for the two vibrational temperatures are shown in Fig. 10. The experimentally determined H-atom density at 1000 μsec for 10% H_2 in H_2-N_2 was $\sim 7\times 10^{13}$ cm^{-3} (see Fig. 8). The estimated H_2 vibrational population in $v=4$ and 5 (see Fig. 10) is approaching this density by 1000 μsec for both initial vibrational temperatures. The experimental H-atom densities for 10% H_2 in H_2-N_2 as a function of pulse duration are shown in Fig. 11 (closed circles joined by solid lines) along with the estimated $H_2, v=4$ and 5, populations for both vibrational temperatures (open squares and triangles respectively, joined by dashed lines). The calculated H_2 vibrational densities have been multiplied by 2 for comparison with the H-atom densities. The experimental H-atom densities are roughly the same as the calculated $H_2, v=5$, density but less than the $v=4$ density for $T_v=3000$ K; for $T_v=3500$ K, however, the vibrational densities for both $H_2, v=4$ and 5, are well above the experimental H-atom densities. From the calculation with the lower initial vibrational temperature, the population in $v=4$ and 5 is just sufficient to account for the experimental H-atom densities, but a near unity reaction probability would be required for every vibrationally excited H_2 and N_2. For the higher vibrational temperature, the vibrational populations are both greater than the experimental H-atom densities, and a reaction probability of $<20\%$ for the vibrationally excited H_2 and N_2 would be sufficient to account for the H-atom density.

TABLE II. Cross sections for H_2 dissociation determined with calculated H_2 vibrational population densities compared to a hard-sphere calculation.

Initial T_v (K)	Cross section (10^{-16} cm^2) (4,10) [a]	(5,8) [a]
3000	13	3
3500	4	0.5
Hard sphere [b]	6	

[a] (v,v') corresponds to H_2 and N_2 vibrational quantum numbers $[H_2(v), N_2(v')]$, respectively.
[b] Hard-sphere cross section calculated with H_2 and N_2 molecular diameters of 2.4 and 3.2 (10^{-8} cm), respectively (from Ref. [35]).

A reaction cross section for the dissociation of H_2 from collisions of vibrationally excited H_2 and N_2 can be determined from the measured rate of H-atom production in 1.0 msec and the calculated vibrational population densities of H_2 and N_2 (the H_2 vibrational populations are from the present calculation, while the N_2 vibrational populations were taken from Gorse and Capitelli [31]). The cross sections were calculated for $H_2, v=4$, with $N_2, v=10$, and $H_2, v=5$, with $N_2, v=8$, for both initial vibrational temperatures and a gas translational temperature of 400 K. The results are given in Table II. Also given is a cross section calculated for a hard-sphere collision of H_2 and N_2 (the molecular diameters used were 2.4 Å for H_2 and 3.2 Å for N_2 [35]). Comparison of the determined cross sections and the hard-sphere cross section shows them to be comparable in size; only the cross section for $H_2, v=5$, and $N_2, v=8$, and an initial $T_v=3000$ K is less than the hard-sphere cross section, while both cross sections are less than the hard-sphere cross section with an initial $T_v=3500$ K. Thus, a H_2 vibrational distribution that is intermediate between the calculated distributions could account for the experimentally determined H atom densities.

V. CONCLUSION

The concentration of H atoms produced in a pulsed dc discharge was measured as a function of discharge pulse duration and gas mixture with constant current and pressure in a H_2-N_2 mixed-gas discharge. The fractional dissociation of H_2 with N_2 dilution changed significantly with pulse duration. The contribution to H_2 dissociation in the discharge from both direct electron impact and heavy-particle energy transfer was determined from the temporal behavior of the H-atom production. For short pulse durations ($\leqslant 100$ μsec),

no enhancement occurred in the fractional dissociation of H_2 with N_2; at longer pulse durations ($\geqslant 500$ μsec), however, the fractional dissociation increased with N_2 concentration. A comparison was made of measured H-atom densities and estimates of the populations of excited vibrational levels in ground state H_2 and N_2 [31] in the discharge. The results showed that vibrationally excited $H_2, v \geqslant 4$, and $N_2, v \geqslant 8$, may be responsible for the H-atom production through heavy-particle energy transfer processes in a short duration pulsed discharge, where heavy-particle energy transfer processes have not reached steady-state equilibrium conditions.

ACKNOWLEDGMENTS

The authors would like to thank Dr. Steve Adams, Dr. Charlie DeJoseph, and Dr. Peter Bletzinger for many useful discussions and Alan Forlines for technical support. One of the authors (J.M.W.) acknowledges support under USAF Contract No. F33615-98-C-2806.

[1] J. Bougdira, G. Henrion, and M. Fabry, J. Phys. D **24**, 1076 (1991).
[2] J. Loureiro and A. Ricard, J. Phys. D **26**, 163 (1993).
[3] A. Ricard, J. Phys. D **30**, 2261 (1997).
[4] S. P. Brühl, M. W. Russel, B. J. Gómez, G. M. Grigioni, J. N. Feugas, and A. Ricard, J. Phys. D **30**, 2917 (1997).
[5] B. J. Gómez, S. P. Brül, J. N. Feugeas, and A. Ricard, J. Phys. D **32**, 1239 (1999).
[6] A. Callegari, P. D. Hoh, D. A. Buchanan, and D. Lacey, Appl. Phys. Lett. **54**, 332 (1989).
[7] A. Paccagnella, A. Callegari, E. Latta, and M. Gasser, Appl. Phys. Lett. **55**, 259 (1989).
[8] A. D. Tserepi, J. R. Dunlop, B. L. Preppernau, and T. A. Miller, J. Vac. Sci. Technol. A **10**, 1188 (1992).
[9] J. Loureiro and C. M. Ferreira, J. Phys. D **22**, 67 (1989).
[10] J. Loureiro and C. M. Ferreira, J. Phys. D **22**, 1680 (1989).
[11] J. Loureiro, Phys. Rev. E **47**, 1262 (1993).
[12] K. Sawada and T. Fujimoto, J. Appl. Phys. **78**, 2913 (1995).
[13] V. Guerra and J. Loureiro, Plasma Sources Sci. Technol. **6**, 361 (1997).
[14] J. Amorim, J. Loureiro, G. Baravian, and M. Touzeau, J. Appl. Phys. **82**, 2795 (1997).
[15] S. D. Benedictis, G. Dilecce, and M. Simek, J. Chem. Phys. **110**, 2947 (1999).
[16] G. Baravian and A. Ricard, in *Proceedings of the 11th International Symposium on Plasma Chemistry*, edited by R. Muntz (Blackwell, Oxford, 1994), pp. 1511–1515.
[17] R. Nagpal and A. Garscadden, Chem. Phys. Lett. **231**, 211 (1994).
[18] A. Garscadden and R. Nagpal, Plasma Sources Sci. Technol. **4**, 268 (1995).
[19] R. Nagpal and A. Garscadden, Contrib. Plasma Phys. **4-5**, 301 (1995).
[20] P. Bletzinger and B. N. Ganguly, Chem. Phys. Lett. **247**, 584 (1995).
[21] J. Amorim, G. Baravian, and A. Ricard, Plasma Chem. Plasma Process. **15**, 721 (1995).
[22] R. Nagpal, B. N. Ganguly, P. Bletzinger, and A. Garscadden, Chem. Phys. Lett. **257**, 386 (1996).
[23] J. Amorim, G. Baravian, and G. Sultan, Appl. Phys. Lett. **68**, 1915 (1996).
[24] B. N. Ganguly and P. Bletzinger, J. Appl. Phys. **82**, 4772 (1997).
[25] B. N. Ganguly and P. Bletzinger, Appl. Phys. Lett. **72**, 1570 (1998).
[26] B. Gordiets, C. M. Ferreira, M. J. Pinheiro, and A. Ricard, Plasma Sources Sci. Technol. **7**, 363 (1998).
[27] B. Gordiets, C. M. Ferreira, M. J. Pinheiro, and A. Ricard, Plasma Sources Sci. Technol. **7**, 379 (1998).
[28] J. R. Dunlop, A. D. Tserepi, B. L. Preppernau, T. N. Cerny, and T. A. Miller, Plasma Chem. Plasma Process. **9**, 157 (1992).
[29] J. Bittner, K. Kohse-Höinghaus, U. Meier, and T. Just, Chem. Phys. Lett. **143**, 571 (1988).
[30] M. Cacciatore, M. Capitelli, and C. Gorse, Chem. Phys. **66**, 141 (1982).
[31] C. Gorse and M. Capitelli, in *Molecular Physics and Hypersonic Flows*, edited by M. Capitelli (Kluwer Academic Publishers, Netherlands, 1996), pp. 437–449.
[32] C. E. Treanor, J. W. Rich, and R. G. Rehm, J. Chem. Phys. **48**, 1798 (1968).
[33] M. Cacciatore, M. Capitelli, S. De Benedictis, M. Dilonardo, and C. Gorse, in *Nonequilibrium Vibrational Kinetics*, edited by M. Capitelli (Springer-Verlag, Berlin, 1986), pp. 5–46.
[34] M. Cacciatore, M. Capitelli, and M. Dilonardo, Chem. Phys. **34**, 193 (1978).
[35] *CRC Handbook of Chemistry and Physics*, 56th ed., edited by R. C. Weast (CRC Press, Cleveland, 1975), p. F-206.